Model Predictive Control of Energy-Stored Quasi-Z-Source Inverter Without Weighting Factor

Tian Lan
Department of Mechanical Engineering
Qinghai University
Qinghai, China
tianlan9308@gmail.com

Yan Zhang
Department of Chemical Machinery
Qinghai University
Qinghai, China
zy210825@163.com

Wanhong Zhang
Department of Chemical Machinery
Qinghai University
Qinghai, China
zwh0511@163.com

***Abstract*—When the quasi-Z-source inverter with energy storage (ES-qZSI) by model predictive control (MPC), an appropriate weighting factor is designed in the cost function to achieve the best possible performance from the system. However, adding weighting factors directly to a cost function produces both numerical instability and computational complexity, in addition to the inability to distinguish between the role of weighting factors and system dynamics in the performance of the relevant system. This paper proposes an improved MPC algorithm without weighting factors for the ES-qZSI system. The computational cost of MPC is significantly reduced by the voltage vector control method without affecting the control performance. Moreover, the inductance current term in the control logic is considered individually, thus eliminating its weighting factor. Compared with conventional MPC, computational efficiency and control performance are demonstrated via numerical simulation. The simulation results show a good dynamic and static performance for the improved algorithm.**

***Index Terms*—MPC, energy storage, weighting factor, quasi-Z-source inverter (qZSI).**

I. Introduction

Energy crises and environmental pollution have become global issues that require urgent resolution. Developing and utilizing renewable energy is an urgent need for the sustainable development of human society. Solar energy, one of the most abundant and cleanest renewable sources, is becoming increasingly popular. The inverter is the core component responsible for converting light energy into electricity, and its structure, cost, and performance play a critical role in the system. The qZSI breaks the limitations of traditional voltage source inverters (VSI) in relevant applications due to its unique impedance source network, which permits two switches on the same bridge arm to conduct simultaneously without damaging the switching devices. The state is known as the shoot-through (ST) state. By reasonably controlling the insertion of the ST state to achieve the DC bus voltage lift regulation of the qZSI network, thus improving the reliability and safety of the system.

Solar power generation is intermittent and vulnerable to environmental factors (temperature, radiation, weather). To ensure the reliability of power supply to customers and to mitigate the impact on grid-connected power quality, battery energy storage (BES) systems effectively compensate for fluctuations in solar power generation by storing redundant energy or filling in shortfalls to obtain stable and smooth power output. Traditional energy storage PV systems typically require the connection of additional DC-DC converters, which makes the system more complex and costly. As a result of connecting the battery parallel to capacitors C_1 or C_2 in the qZSI network, the ES-qZSI system can achieve optimal power control at three ends of the photovoltaic(PV) battery, energy storage device, and grid/load without requiring additional converters and charge/discharge loops to achieve energy storage [1], [2]. Assuming that there are no system losses, the voltages across capacitors C_1 and C_2 satisfy the following equation:

$$\begin{cases} v_{C1} = \dfrac{1-D}{1-2D} v_{in} \\ v_{C2} = \dfrac{D}{1-2D} v_{in} \end{cases} \tag{1}$$

Here D is the ST duty ratio, v_{in} is DC source voltage. For the energy storage quasi-Z-source network to achieve boost function, it is necessary to satisfy D: 0<D<0.5. As seen from equation (1), a parallel connection of the battery and capacitor C_1 results in a more extensive power compensation range and a higher battery voltage level than a parallel connection of the battery and capacitor C_2 [3].

Adding a BES system to a qZSI circuit increases the complexity of system operation and analysis. In order to control multiple variables, conventional linear control typically requires using a complex modulator with nested loops. As a result, there are limitations concerning dynamic response, constraint handling, controller design, and stability. With the development of microprocessors and the increase in computing power, some nonlinear control algorithms have been applied to the qZSI system, including neural network control [4], fuzzy control [5], and sliding mode control [6]. Compared to conventional linear control algorithms, these algorithms provide a faster dynamic response but also increase the complexity of the controller design, requiring PWM generators inevitably [7].

Over the past few years, MPC has become widely used in power electronics as an advanced control method. As a type of MPC, finite control set model predictive control (FCS-MPC) has received considerable academic attention due to its ease of achieving multi-objective constrained optimal

978-1-6654-0984-1/22/$31.00 ©2022 IEEE

control and Fast-tracking response [8]–[10]. Various MPC methods have been applied to qZSI systems in the literature [11]–[13], which do not require modulation techniques and are, therefore, more reliable and flexible than other methods. However, FCS-MPC still has some unavoidable drawbacks; the weighting coefficients are difficult to design, the computational burden is relatively high, the control accuracy is inferior, and the switching frequency is not fixed. A low-computation control algorithm for ES-qZSI systems is proposed in the literature [14], combining MPC and proportional resonant (PR) controllers, reducing the number of controller iterations and the computational burden. Literature [15] suggests combining MPC with direct power control in the ES-qZSI system to reduce switching losses by fixing switching frequency.

Based on the above analysis, the study presents an MPC strategy without weighting factors for ES-qZSI. This method consists of two steps: As a first step, the control logic controls the inductor current independently, which provides a basis for evaluating system state selection; Secondly, the voltage vector control method is used in order to minimize the number of calculations needed to calculate the cost function. By combining these two steps, the FCS-MPC cost function is simplified, the calculation time is reduced, and the performance of the control system is enhanced. Based on the simulation results, the proposed control strategy proved effective.

The following is the organization of this paper. An overview of the topology and operating principle of the ES-qZSI circuit is presented in Section II, followed by the development of the corresponding prediction model. In Section III, the proposed MPC strategy is discussed in more detail. In section IV, the simulation results of the proposed control strategy are presented, and in section V, the paper is concluded.

II. MODEL AND ANALYSIS OF ES-QZSI

A. Operational Principles of ES-qZSI

Fig. 1 illustrates the ES-qZSI system consisting of inductors L_1 and L_2, capacitors C_1 and C_2, diode D, a resistance inductance (RL) load, a three-phase inverter, and an energy storage battery BT connected in parallel at both ends of C_1. As with the qZSI, the ES-qZSI system has two operating states in a steady state: the ST state and the non-shoot-through (NST) state. Fig. 2 illustrates the equivalent circuit on the DC side. According to Fig. 2(a), in the ST state, the diode turn-off, and

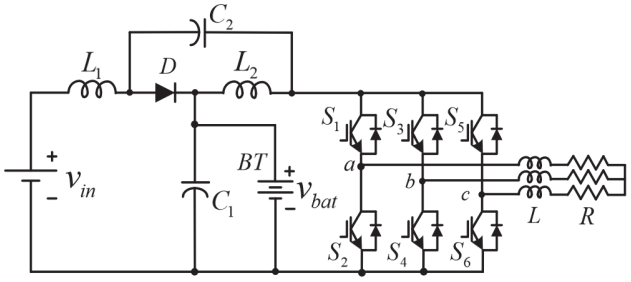

Fig. 1. ES-qZSI with a RL load.

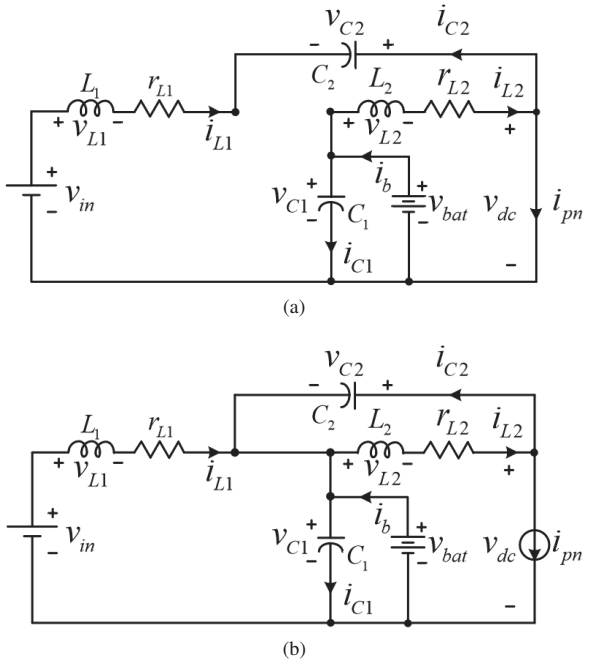

Fig. 2. Equivalent circuit for the DC side. (a) ST state (b) NST state.

the PV cell and capacitor charge the inductor simultaneously. The DC link voltage v_{dc} is zero. An NST state is illustrated in Fig. 2(b), where the diode turns on, the PV cell and inductor provide power to the capacitor simultaneously, while the AC side loads receive additional power. The third power supply automatically balances the power difference when two power supplies are controlled simultaneously. Without considering the system power loss, the power balance equation is as follows:

$$P_{pv} + P_b = P_{out} \tag{2}$$

According to equation (2), P_{pv} represents the output power of the PV cell and is positive. P_{out} indicates the output power of the AC side. When P_{out} = P_{pv}, the battery does not participate in energy exchange; at this time, the battery is neither charged nor discharged, battery power P_b = 0, and battery current i_b = 0. When $P_{out} > P_{pv}$, the battery is discharged, $P_b > 0$, and $i_b > 0$. When $P_{out} < P_{pv}$, the battery is charged, $P_b < 0$, and $i_b < 0$. As part of this paper, we will model and analyze the AC side separately from the DC side.

B. DC side model

The dynamic equations take different forms depending on the system's state (ST or NST).

1) shoot-through state: As shown in equation (3), the kinetic equations of the DC side of the ES-qZSI system in the ST state are derived according to the Kirchhoff voltage (KVL) and current (KCL) laws.

$$\begin{cases} L_1 \dfrac{\mathrm{d}i_{L1}}{\mathrm{d}t} = v_{in} + v_{C2} - r_{L1} i_{L1} \\ L_2 \dfrac{\mathrm{d}i_{L2}}{\mathrm{d}t} = v_{C1} - r_{L2} i_{L2} \\ C_1 \dfrac{\mathrm{d}v_{C1}}{\mathrm{d}t} = i_b - i_{L2} \\ C_2 \dfrac{\mathrm{d}v_{C2}}{\mathrm{d}t} = -i_{L1} \end{cases} \tag{3}$$

The values of v_{C1}, v_{C2}, i_{L1}, i_{L2}, r_{L1}, and r_{L2} represent the voltages across the capacitors C_1 and C_2, the currents through the inductors L_1 and L_2, and the stray resistances of the inductors.

The future behavior of the control variables is predicted in the MPC algorithm by using a discrete-time model. In order to obtain the discrete-time model, the Forward Euler method is often applied, which can be defined as follows:

$$\frac{\mathrm{d}x}{\mathrm{d}t} = \frac{x(k+1) - x(k)}{T_s} \tag{4}$$

Here T_s is the sampling time, and Equation (5) shows the predicted value of the inductor current at the moment $k+1$ under the ST state condition.

$$\begin{aligned} i^p_{L1ST}(k+1) =& (1 - \frac{r_{L1} T_s}{L_1}) i_{L1}(k) \\ &+ \frac{T_s}{L_1}(v_{in}(k) + v_{C2}(k)) \end{aligned} \tag{5}$$

2) non-shoot-through state: In the NST state, the kinetic equations of the DC side of the ES-qZSI system can be derived according to KVL and KCL.

$$\begin{cases} L_1 \dfrac{\mathrm{d}i_{L1}}{\mathrm{d}t} = v_{in} - v_{C1} - r_{L1} i_{L1} \\ L_2 \dfrac{\mathrm{d}i_{L2}}{\mathrm{d}t} = -v_{C2} - r_{L2} i_{L2} \\ C_1 \dfrac{\mathrm{d}v_{C1}}{\mathrm{d}t} = i_b + i_{L1} - i_{pn} \\ C_2 \dfrac{\mathrm{d}v_{C2}}{\mathrm{d}t} = i_{L2} - i_{pn} \end{cases} \tag{6}$$

In the NST state, equation (7) predicts the inductor current at $k+1$.

$$\begin{aligned} i^p_{L1NST}(k+1) =& (1 - \frac{r_{L1} T_s}{L_1}) i_{L1}(k) \\ &+ \frac{T_s}{L_1}(v_{in}(k) - v_{C1}(k)) \end{aligned} \tag{7}$$

C. AC side model

The three-phase inverter has fifteen valid switch configurations. These include six active states, two null states, and seven ST states. The same output voltage vector will be generated in the null and ST states so that it can be simplified to one configuration per state. As a result of this simplified method, the calculation time will be significantly reduced. In order to facilitate the following analysis, the switch function $S_n (n = 1, 2, ...6)$ is defined as follows:

TABLE I
SWITCHING STATES AND OUTPUT VOLTAGE SPACE VECTORS

States	S_1	S_2	S_3	S_4	S_5	S_6	Voltage vector
NST	0	1	0	1	0	1	v_0
	1	0	0	1	0	1	v_1
	1	0	1	0	0	1	v_2
	0	1	1	0	0	1	v_3
	0	1	1	0	1	0	v_4
	0	1	0	1	1	0	v_5
	1	0	0	1	1	0	v_6
ST	1	1	1	1	1	1	v_7

$$S_n = \begin{cases} 1 & \textit{Switch on} \\ 0 & \textit{Switch off} \end{cases} \tag{8}$$

In Table.I, eight simplified switch combinations are listed, and different combinations will result in different voltage vectors. In addition, the output voltage space vector is shown in equation (9).

$$v_x = \frac{2}{3} v_{dc}(S_a + \alpha S_b + \alpha^2 S_c) \tag{9}$$

where α=$exp(j2\pi/3)$, x = [0,1,...7], v_{dc} represents the DC link voltage, and S_a, S_b, and S_c denote the switching states for phases a, b, and c, respectively.

As shown in Fig. 1, when the equivalent circuit for the load consists of a resistor and an inductor, the dynamic equation for the load is as follows:

$$L\frac{di}{dt} = v - Ri \tag{10}$$

As shown in this equation, the load current of the ES-qZSI is indicated by i. The inductance and resistance of the AC side are given by L and R, respectively. Inverters generate voltage vectors, represented by v. It is possible to replace the load current derivative term di/dt with the forward Euler approximation. As a result, equation (11) provides the discrete-time expression of equation (10).

$$i(k+1) = (1 - \frac{RT_s}{L}) i(k) + \frac{T_s}{L} v(k) \tag{11}$$

According to Equation (11), the load current $i(k+1)$ at the moment $k+1$ is determined both by the inverter voltage $v(k)$ and the load current $i(k)$. It is clear from Table.I that there exist eight voltage vectors that can be used as the output voltage of the inverter. Therefore, the predicted value of the load current at the moment $k+1$ is as follows.

$$i^p_x(k+1) = (1 - \frac{RT_s}{L}) i(k) + \frac{T_s}{L} v_x(k) \tag{12}$$

III. PROPOSED MPC ALGORITHM FOR ES-QZSI

Fig. 3 illustrates a detailed example of a predictive control strategy. In Fig. 3(a), load current i_α and its references i^*_α are

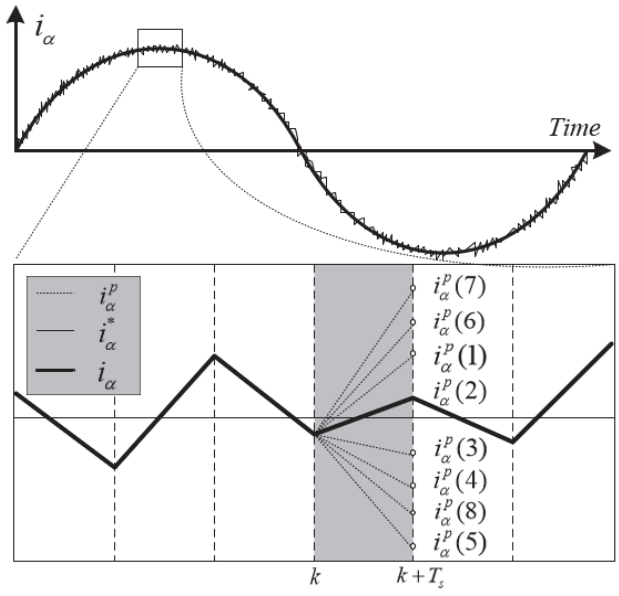

(a)

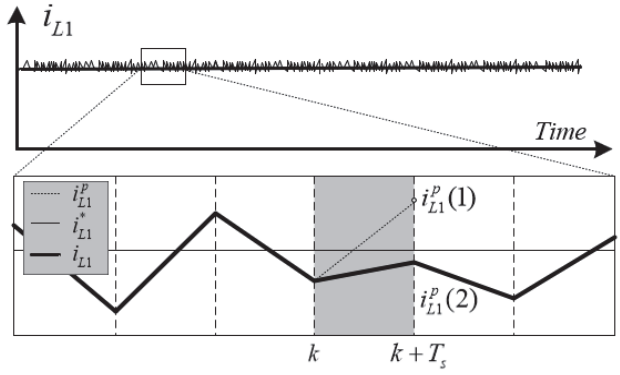

(b)

Fig. 3. Schematic diagram of predicted observation (a) load current (b) inductor current

shown for an entire reference period. Coordinate transformation converts the injected grid current from (A, B, C) to (α, β). Assuming that the predicted value of the real part of the load current is $i_\alpha^p(x)$, it can be seen from Fig. 3(a) that $i_\alpha^p(2)$ is closest to the reference value. The optimizer will choose this state as the best state for the real part of the load current. Similar steps will be followed for the imaginary part (i_β)

For the purpose of measuring the distance between any state and the reference, a cost function (g) is used with a unity weighting factor. Thus, the following is the definition of the load current cost function:

$$\begin{aligned} g_i(k+1) = &|i_\alpha^*(k+1) - i_\alpha^p(k+1)| \\ &+ \left|i_\beta^*(k+1) - i_\beta^p(k+1)\right| \end{aligned} \tag{13}$$

where the real and imaginary components of the reference load current are $i_\alpha^*(k+1)$ and $i_\beta^*(k+1)$, and the real and imaginary parts of the predicted load current are $i_\alpha^p(k+1)$ and $i_\beta^p(k+1)$.

According to equations (5) and (7), Fig. 3(b) illustrates the two current predictions for inductor L_1. The cost function of the inductor current is as follows.

$$g_{i_{L1}}(k+1) = |i_{L1}^*(k+1) - i_{L1}^p(k+1)| \tag{14}$$

The predicted and reference values of the inductance current are $i_{L1}^p(k+1)$ and $i_{L1}^*(k+1)$, respectively.

Due to the unique topology of the ES-qZSI, the voltage across capacitor C_1 equals the battery voltage and does not change during switching. Therefore, the total cost function g consists of two components, the current inductor term ($g_{i_{L1}}$) and the current load term (g_i), to effectively control the ES-qZSI DC link voltage and load current. The total cost function of the system is as follows:

$$\begin{aligned} g(k+1) = &|i_\alpha^*(k+1) - i_\alpha^p(k+1)| \\ &+ \left|i_\beta^*(k+1) - i_\beta^p(k+1)\right| \\ &+ \lambda_1 |i_{L1}^*(k+1) - i_{L1}^p(k+1)| \end{aligned} \tag{15}$$

In this case, λ_1 represents the weighting factor of the inductor current.

According to the current literature on MPC, the strict mathematical method for determining the weighting factor is not clearly defined. The weighting factors are adjusted by trial-and-error, which requires much time and effort.

By selecting the voltage vector v_x, traditional MPC attempts to predict the load current $i(k+1)$ as close as possible to its reference value $i^*(k+1)$. Changing $i(k+1)$ to $i^*(k+1)$ in (11) and rearranging the equation yields:

$$v^*(k) = \frac{L}{T_s}(i^*(k+1) - i(k)) + Ri(k) \tag{16}$$

If the voltage acting on the inverter at time k is equal to $v^*(k)$, then the load current $i(k+1)$ will equal its reference value $i^*(k+1)$, as shown in equation (16). In this case, $v^*(k)$ represents the "required voltage vector" [16]. Fig. 4 illustrates the spatial distribution of the "required voltage vector" and eight voltage vectors. According to this method, the switching state of the inverter at time instant k is determined by choosing which voltage vector approaches the "required voltage vector"$v^*(k)$. In the case of the voltage vector control method, the cost function is as follows:

$$g_x(k+1) = |v^*(k) - v_x(k)| \tag{17}$$

In the following equations (18) and (19), the mathematical expressions of the traditional and improved MPC applied to the inverter are summarized:

$$\begin{cases} i_x^p(k+1) = (1 - \dfrac{RT_s}{L})i(k) + \dfrac{T_s}{L}v_x(k) \\ g_x(k+1) = |i^*(k+1) - i_x^p(k+1)| \\ switch = min\{g_x(k+1)\} \end{cases} \tag{18}$$

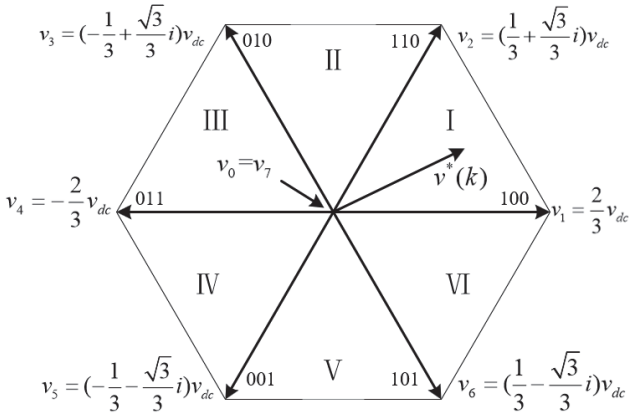

Fig. 4. Voltage vectors for the ES-qZSI.

$$\begin{cases} v^*(k)=\dfrac{L}{T_s}(i^*(k+1)-i(k))+Ri(k) \\ g_x(k+1)=|v^*(k)-v_x(k)| \\ switch=min\{g_x(k+1)\} \end{cases} \tag{19}$$

It is possible to prove that (18) and (19) are equivalent by substituting (12) into (19) and rearranging the equation. As shown in (20), the simplified equation is as follows:

$$\begin{cases} i^p(k+1)=(1-\dfrac{RT_s}{L})i(k)+\dfrac{T_s}{L}v_x(k) \\ g_x(k+1)=\delta\,|i^*(k+1)-i_x^p(k+1)| \\ switch=min\{g_x(k+1)\} \end{cases} \tag{20}$$

where $\delta=(L/T_s)$.

The difference between equations (18) and (20) is that the multiplication factor in the cost function differs. However, their performance is the same. Fig. 5 and Fig. 6 illustrate the flowcharts of the conventional and improved MPC algorithms. The ST or NST state is determined by the predicted value of the inductor current. Accordingly, the discriminant for the inductor current sub-cost function is:

$$\begin{aligned} \Delta=&|i_{L1}^*(k+1)-i_{L1ST}^p(k+1)|- \\ &|i_{L1}^*(k+1)-i_{L1NST}^p(k+1)| \end{aligned} \tag{21}$$

The ST state is determined by equation (21). If $\Delta<0$, the ST state is selected, and the corresponding switch state is output directly as the optimal switch state without checking the other seven states; if $\Delta>0$, the NST state is selected, and an inner loop is used to optimize the optimal switch state. Assume that there are two NST states and one ST state in three continuous control cycles. Table.II compares the calculation time for each equation for the two MPC algorithms. The improved MPC algorithm reduces the computational effort by 68% compared with the traditional MPC algorithm, significantly improving computational efficiency.

IV. SIMULATION RESULTS

MATLAB/Simulink was used to simulate the ES-qZSI system in order to assess the effectiveness of the improved MPC strategy. The PV module tracks its maximum power point voltage using the MPPT algorithm (The P&O algorithm is used in this paper) and obtains the reference voltage v_{inref}. The difference between the actual voltage v_{in} and the reference voltage v_{inref} is used to calculate the output reference current i_{pvref} of the PV panel through the PI regulator. Thus, in the steady state, i_{pvref}=i_{L1ref} is used as a reference value for the current in the inductance L_1, which tracks the PV power output. Equation(22) shows how the reference power indirectly determines the reference load current. The parameters of the

TABLE II
SWITCHING STATES AND VOLTAGE VECTORS

Equation	(5)	(7)	(12)	(15)	(16)	(17)	Total
Traditional algorithm	1×3	7×3	8×3	8×3	–	–	**72**
Proposed algorithm	1×3	1×3	–	–	1×3	7×2	**23**

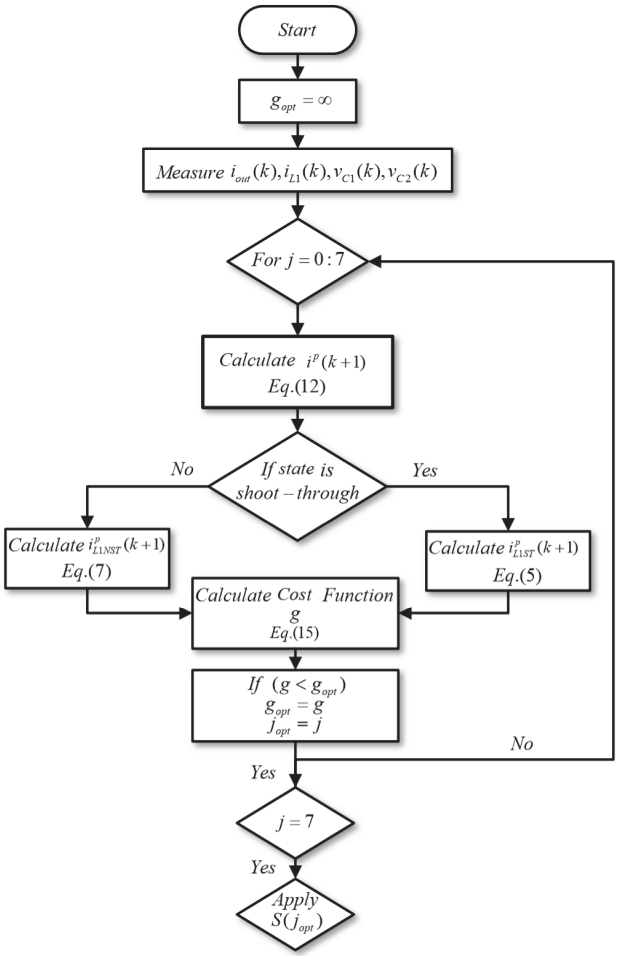

Fig. 5. Flowchart of the conventional MPC algorithm.

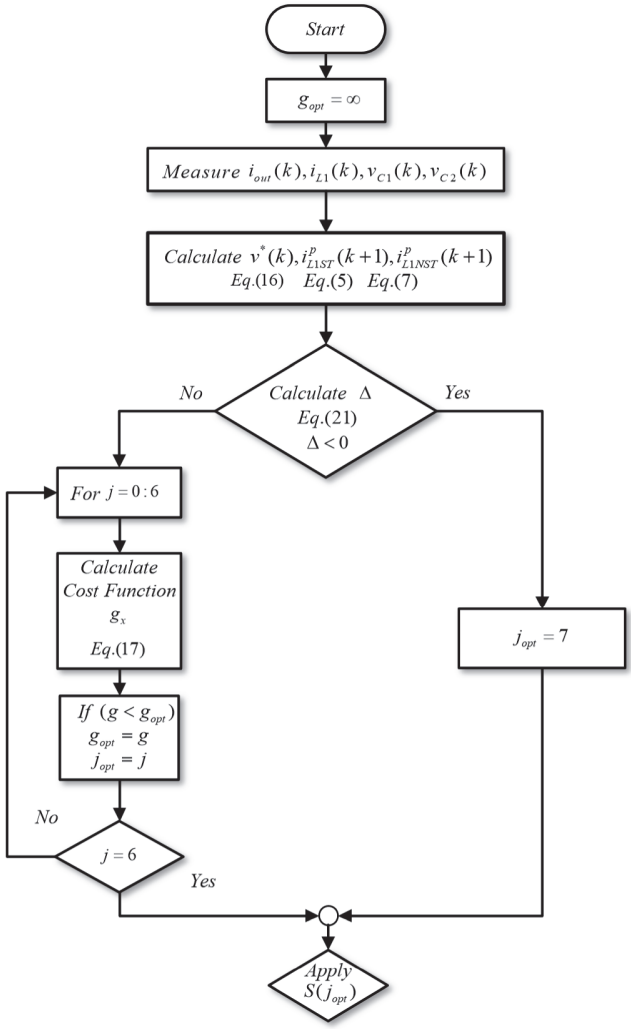

Fig. 6. Flowchart of the proposed MPC algorithm.

system are shown in Table.III and Table.IV.

$$i_{out\_ref} = \sqrt{\frac{2P_{out\_ref}}{3R}} \tag{22}$$

A. Photovoltaic Power Fluctuation

Initially, it is necessary to examine the stability and dynamic performance of the system when the PV power fluctuates. The ambient temperature will be assumed to be $25°C$. Load power consumption is set at 240W. Initial PV power is 158W,

TABLE III
SPECIFICATIONS OF PV ARRAY PANEL SUNPOWER SPR-360 UNDER STANDARD TEST CONDITION ($25°C, 1000W/m^2$)

Parameter	Symbol	Value
Maximum Power	P_{mp}	359.919W
Voltage at maximum power point	V_{mp}	59.1V
Current at maximum power point	I_{mp}	6.09A

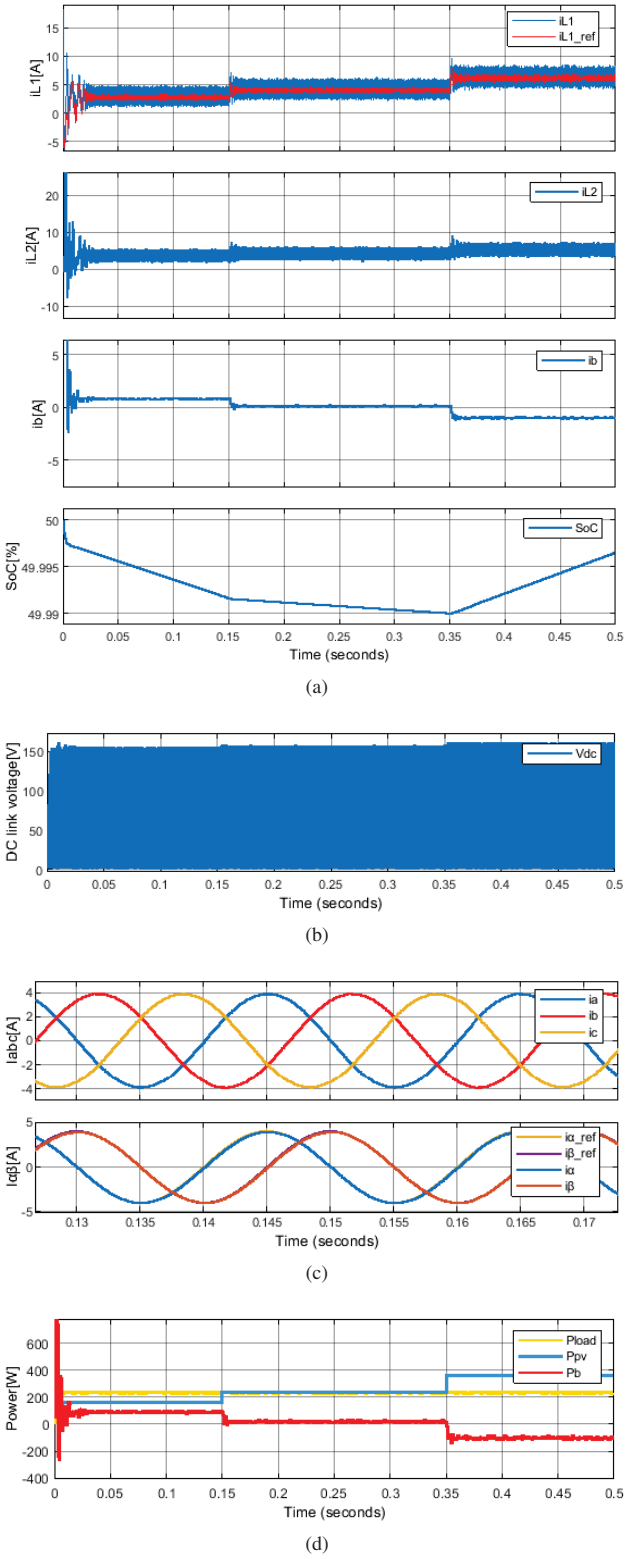

Fig. 7. Simulation results under PV power fluctuation. (a) the inductor currents of the qZSI network, the battery current, and the SoC of the battery. (b) DC link voltage (c) Three-phase currents. (d) System power diagrams

TABLE IV
SYSTEM PARAMETERS

Parameter	Symbol	Value
Battery voltage	v_{bat}	100V
Load inductance	L	24μH
Load resistance	R	10Ω
qZSI inductors	L_1, L_2	600μH
qZSI capacitors	C_1, C_2	470μF
Resistance of inductors	r_{L1}, r_{L2}	0.1Ω
Sample time	T_s	10μSec

increasing to 240W at 0.15s, and 360W at 0.35s. PV power cannot meet load-side power demands during 0∼0.15s. In order to ensure system output power remains stable, the battery discharges, and the State of Charge (SoC) of the battery drops from 49.975% to approximately 49.167%.

PV power meets the load-side power demand within 0.15s to 0.35s. The battery is neither discharged nor charged when system power consumption is ignored. However, Fig. 7(a) indicates that the SoC is slightly reduced during 0.15∼0.35s. As a result, we can conclude that the ripple in battery current will also affect SoC, and the impact will gradually increase with the long-term operation of the system [17].

In the period of 0.35 to 0.5s, PV power exceeds the load power demand. SoC increases from 49.9901% to 49.9965% as the storage battery absorbs additional energy.

Fig. 7(a) illustrates the changes in inductor currents i_{L1}, i_{L2}, and battery current i_b as the PV power changes. i_{L1} quickly and accurately tracks the change in the reference value i_{L1ref} at 0.15s and 0.35s. In Fig. 7(c), the three-phase load current i_{abc} is less affected by PV power fluctuations, ensuring constant load power. In Fig. 7(d), the system power flow is shown during the dynamics.

B. Load Power Fluctuation

Fig. 8 illustrates the simulation results when the output power is changed. PV power output remains constant at 270W (solar panel temperature T=25$^\circ C$ and solar irradiance G=750W/m^2). The output power increases instantly from 200W to 360W at 0.2 seconds. To maintain the power balance between the systems, the battery is switched from charging to discharging.

Fig. 8(a) illustrates that the current reference value for the inductor current remains at 4.5A as the load power changes. Fig. 8(c) also shows the change in peak load current from 3.6A to 4.9A at 0.2 sec. The load current accurately and quickly tracks the sinusoidal reference. The proposed predictive control strategy has been demonstrated to have high track quality.

C. Total Harmonic Distortion

According to Fig. 9, the load current total harmonic distortion (THD) under the traditional MPC strategy is approximately 0.87%, whereas the THD under the improved MPC strategy is about 0.60%, which is a 31% reduction compared to the conventional algorithm. With the proposed MPC algorithm,

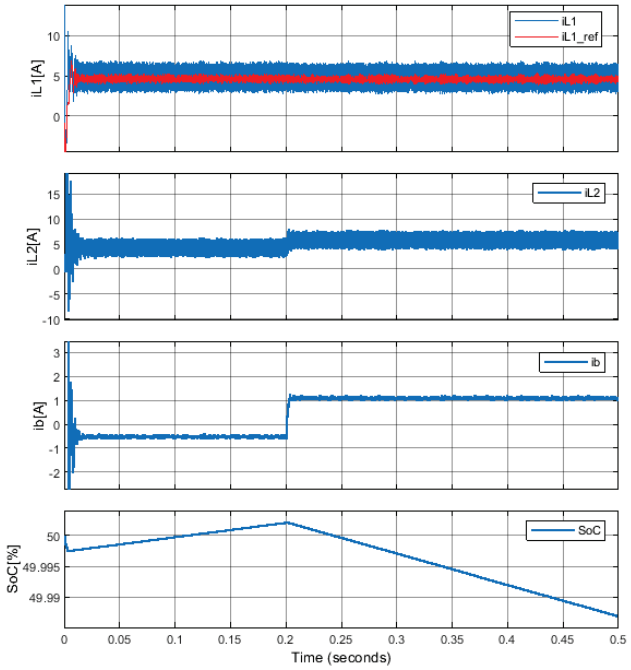

(a)

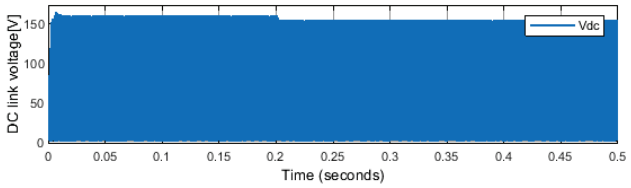

(b)

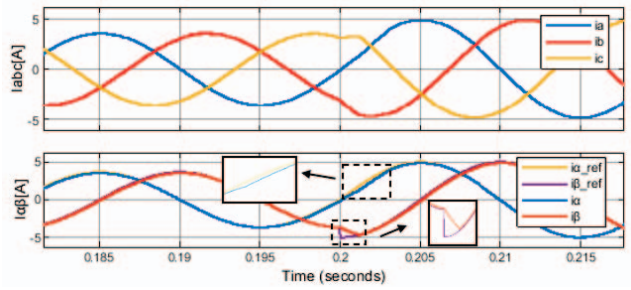

(c)

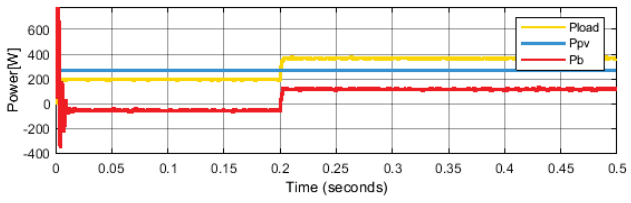

(d)

Fig. 8. Simulation results under load power fluctuation. (a) the inductor currents of the qZSI network, the battery current, and the SoC of the battery. (b) DC link voltage (c) Three-phase currents. (d) System power diagrams

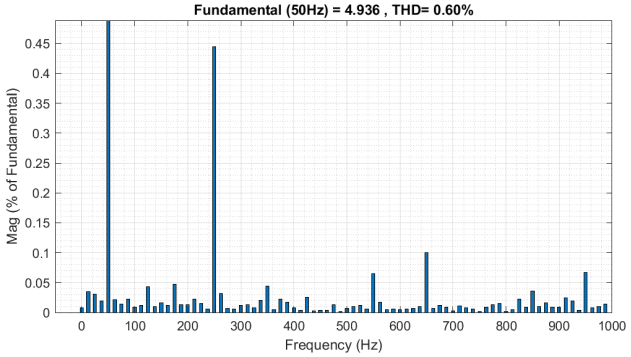

(a)

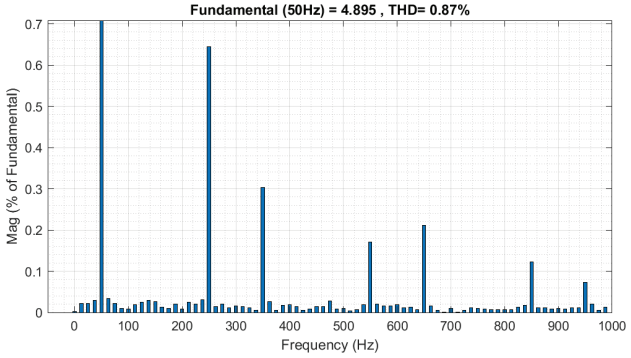

(b)

Fig. 9. Load current harmonic spectrum. (a) Improved MPC algorithm. (b) Conventional MPC algorithm.

the control strategy is simplified, and a large number of calculation processes are avoided. At the same frequency, the output load current ripple is lower, and the tracking quality is improved.

V. CONCLUSION

This paper proposes an MPC strategy without a weighting factor for ES-qZSI. A new control structure is designed. In the control logic, the inductor currents are controlled independently, and the ST and NST states are selected in advance, thus saving loop calculations and eliminating the weighting factor. Additionally, the voltage vector selection method is used to simplify the cost function and reduce the time required to operate the system. Notably, the proposed improved MPC strategy exhibits excellent performance in reducing the THD for the load current and reducing the computational effort required. Based on simulation results, the proposed MPC scheme has good dynamic and static performance.

ACKNOWLEDGMENT

This work was supported in part by the National Natural Science Foundation of China under Grant 61741115 and the Qinghai Department of Science and Technology under Grant 2017-ZJ-953Q.

REFERENCES

[1] B. Ge et al., "An Energy-Stored Quasi-Z-Source Inverter for Application to Photovoltaic Power System," in IEEE Transactions on Industrial Electronics, vol. 60, no. 10, pp. 4468-4481, Oct. 2013.

[2] Y. Liu, B. Ge, H. Abu-Rub and F. Z. Peng, "Control System Design of Battery-Assisted Quasi-Z-Source Inverter for Grid-Tie Photovoltaic Power Generation," in IEEE Transactions on Sustainable Energy, vol. 4, no. 4, pp. 994-1001, Oct. 2013.

[3] B. Ge, Y. Liu, H. Abu-Rub and F. Z. Peng, "State-of-Charge Balancing Control for a Battery-Energy-Stored Quasi-Z-Source Cascaded-Multilevel-Inverter-Based Photovoltaic Power System," in IEEE Transactions on Industrial Electronics, vol. 65, no. 3, pp. 2268-2279, March 2018.

[4] H. Rostami and D. A. Khaburi, "Neural networks controlling for both the DC boost and AC output voltage of Z-source inverter," 2010 1st Power Electronic & Drive Systems & Technologies Conference (PEDSTC), 2010, pp. 135-140.

[5] B. Hamed and N. A. Qaoud, "Fuzzy Control Design for Quasi-Z-Source Three Phase Inverter," 2019 IEEE 7th Palestinian International Conference on Electrical and Computer Engineering (PICECE), 2019, pp. 1-6.

[6] B. Xu and X. Ran, "Sliding Mode Control for Three-Phase Quasi-Z-Source Inverter," in IEEE Access, vol. 6, pp. 60318-60328, 2018.

[7] Y. Liu, X. Liu, X. Li, H. Yuan and Y. Xue, "Model Predictive Control of Dual-Mode Energy-Stored Quasi-Z-Source Photovoltaic System," 2022 3rd International Conference on Smart Grid and Renewable Energy (SGRE), 2022, pp. 1-6.

[8] S. Vazquez, J. Rodriguez, M. Rivera, L. G. Franquelo and M. Norambuena, "Model Predictive Control for Power Converters and Drives: Advances and Trends," in IEEE Transactions on Industrial Electronics, vol. 64, no. 2, pp. 935-947, Feb. 2017.

[9] S. Kouro, M. A. Perez, J. Rodriguez, A. M. Llor and H. A. Young, "Model Predictive Control: MPC's Role in the Evolution of Power Electronics," in IEEE Industrial Electronics Magazine, vol. 9, no. 4, pp. 8-21, Dec. 2015.

[10] P. Karamanakos and T. Geyer, "Guidelines for the Design of Finite Control Set Model Predictive Controllers," in IEEE Transactions on Power Electronics, vol. 35, no. 7, pp. 7434-7450, July 2020.

[11] A. Ayad, P. Karamanakos and R. Kennel, "Direct Model Predictive Current Control Strategy of Quasi-Z-Source Inverters," in IEEE Transactions on Power Electronics, vol. 32, no. 7, pp. 5786-5801, July 2017.

[12] A. Bakeer, M. A. Ismeil and M. Orabi, "A Powerful Finite Control Set-Model Predictive Control Algorithm for Quasi Z-Source Inverter," in IEEE Transactions on Industrial Informatics, vol. 12, no. 4, pp. 1371-1379, Aug. 2016.

[13] M. Mosa, R. S. Balog and H. Abu-Rub, "High-Performance Predictive Control of Quasi-Impedance Source Inverter," in IEEE Transactions on Power Electronics, vol. 32, no. 4, pp. 3251-3262, April 2017.

[14] A. Lashab, D. Sera and J. M. Guerrero, "A Low-Computational High-Performance Model Predictive Control of Single Phase Battery Assisted Quasi Z-Source PV Inverters," 2019 10th International Conference on Power Electronics and ECCE Asia (ICPE 2019 - ECCE Asia), 2019, pp. 1873-1878.

[15] Tang M, Yang S, Zhang K, et al. Model predictive direct power control of energy storage quasi-Z-source grid-connected inverter[J]. Archives of Electrical Engineering, 2022: 21-35.

[16] C. Xia, T. Liu, T. Shi and Z. Song, "A Simplified Finite-Control-Set Model-Predictive Control for Power Converters," in IEEE Transactions on Industrial Informatics, vol. 10, no. 2, pp. 991-1002, May 2014.

[17] A. Lashab, D. Sera, J. Martins and J. M. Guerrero, "Model Predictive-Based Direct Battery Control in PV Fed Quasi Z-Source Inverters," 2018 5th International Symposium on Environment-Friendly Energies and Applications (EFEA), 2018, pp. 1-6.